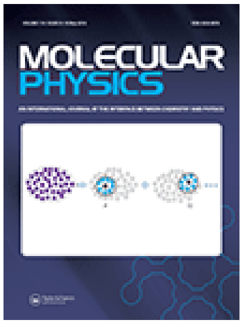

Taylor & Francis
Taylor & Francis Group

Molecular Physics
An International Journal at the Interface Between Chemistry and Physics

ISSN: (Print) (Online) Journal homepage: https://www.tandfonline.com/loi/tmph20

Self-organisation of rhombitruncated cuboctahedral hexagonal columns from an amphiphilic Janus dendrimer

Ning Huang, Qi Xiao, Mihai Peterca, Xiangbing Zeng & Virgil Percec

To cite this article: Ning Huang, Qi Xiao, Mihai Peterca, Xiangbing Zeng & Virgil Percec (2021): Self-organisation of rhombitruncated cuboctahedral hexagonal columns from an amphiphilic Janus dendrimer, Molecular Physics, DOI: 10.1080/00268976.2021.1902586

To link to this article: https://doi.org/10.1080/00268976.2021.1902586

MOLECULAR PHYSICS e1902586
https://doi.org/10.1080/00268976.2021.1902586

Taylor & Francis
Taylor & Francis Group

KLEIN SPECIAL ISSUE

Self-organisation of rhombitruncated cuboctahedral hexagonal columns from an amphiphilic Janus dendrimer*

Ning Huang [a], Qi Xiao [a], Mihai Peterca [a], Xiangbing Zeng [b] and Virgil Percec [a]

[a] Roy & Diana Vagelos Laboratories, Department of Chemistry, University of Pennsylvania, Philadelphia, PA, USA; [b] Department of Materials Science and Engineering, University of Sheffield, Sheffield, UK

ABSTRACT

Frank-Kasper phases are available in both hard and soft complex matter. They have been discovered in metal alloys and subsequently in self-organisations of supramolecular spheres from self-assembling dendrons, dendrimers and dendronized polymers. Recently, they were found in block copolymers, lipids, surfactants, giant surfactants, nanoparticles, DNA particles and even in condensed small molecules such as N_2, O_2, and CO. Here we report the discovery of an amphiphilic Janus dendrimer, that self-assembles in water into vesicles known as dendrimersomes, self-organised also in bulk state into helical columns and spheres forming columnar hexagonal and a Frank-Kasper A15 phase known as $Pm\bar{3}n$. These self-organisations display a *supramolecular orientational memory* (SOM) effect that is induced by an epitaxial nucleation at the transition from columns to spheres and during the reverse process. This SOM effect is mediated by the closed contact supramolecular spheres from the A15 phase. In this case a rhombitruncated cuboctahedral hexagonal columnar arrangement, that to the best of our knowledge is not known in biology or synthetic chemistry, was self-organised. We believe that the addition of amphiphilic Janus dendrimers to the classes of molecules displaying Frank-Kasper phases and the SOM effect will broaden our ability to discover additional complex soft condensed matter morphologies.

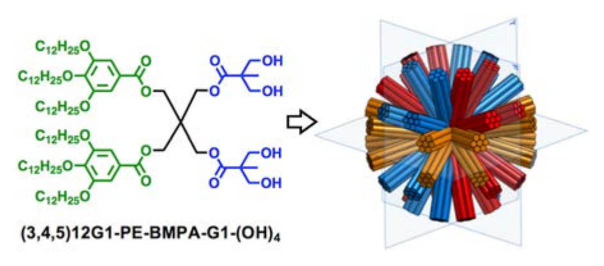

ARTICLE HISTORY
Received 24 January 2021
Accepted 5 March 2021

KEYWORDS
Janus dendrimer; Frank-Kasper phases; supramolecular orientational memory; complex architecture

1. Introduction

During the 1950s, Frank and Kasper introduced a framework to describe metallurgic crystal structures [1,2]. This strategy organised the local packing of spherical metal atoms by a polyhedral coordination sphere of 12, 14, 15 or 16 other atoms. Different combinations of polyhedral coordination give rise to a diversity of Frank-Kasper (F-K) phases. Among the F-K phases observed in metal alloys are the A15 and the σ phases [3,4], which are periodic approximants of dodecagonal liquid quasicrystals [4–7]. F-K phases were subsequently discovered in self-assembling dendrimers and self-organizable dendronized polymers by methodologies involving X-ray diffraction including isomorphous replacement [8–11], transmission electron and optical microscopy [12], solid state NMR [13], and computation [14,15]. Numerous examples of F-K phases in supramolecular dendrimers [16,17] were discovered *via* generational libraries [18–30] and by a deconstruction library strategy [31]. The A15, σ, and other F-K phases have since been discovered also in block copolymers [32–35], surfactants [36–39], giant surfactants [40–44],

---

CONTACT Virgil Percec ✉ percec@sas.upenn.edu Roy & Diana Vagelos Laboratories, Department of Chemistry, University of Pennsylvania, Philadelphia, PA 19104-6323, USA

*Dedicated to the 80th Birthday of Professor Michael L. Klein.

Supplemental data for this article can be accessed here. https://doi.org/10.1080/00268976.2021.1902586

lipids [45,46], inorganic nanoparticles [47,48], DNA particles [49], sugar-polyolefin block-copolymers [50,51], and even in condensed gases such as O_2 [52–55], CO [56], and N_2 [56–61]. The space groups of these phases are most frequently the alternative preferred terminology ($Pm\bar{3}n \equiv$ A15, and $P4_2/mnm \equiv \sigma$) [45].

Out of these many classes of self-assembling molecules, self-assembling dendrons and dendrimers together with self-organizable dendronized polymers seem to be the most suitable to provide a molecular level approach to the elucidation of the mechanism of self-organisation. Theoretical investigations have also contributed to the development of this field [14–17].

Supramolecular orientational memory (SOM) effect provides a new methodology to self-organize unprecedentedly complex morphologies by employing an epitaxial nucleation of the transition from supramolecular columns to spheres and the reverse process. This epitaxial nucleation is mediated by the close contact spheres from the unit cell of the F-K phase. A crown dendron/dendrimer conformation favours this SOM process [62–65]. Here we report that amphiphilic Janus dendrimers that represent a new class of lipids that self-organize in water into biological membrane mimics known as dendrimersomes [66–73] join the above-mentioned classes of self-assembling building blocks and generate F-K phases in bulk state. When the hydrophilic parts of these Janus dendrimers contain H-bonding groups, they form supramolecular crowns that generate helical columns and spheres [74–100]. The amphiphilic Janus dendrimer (3,4,5)12G1-PE-BMPA-G1-$(OH)_4$ selected and investigated here [66,68] exhibits a SOM effect that mediates the self-organisation of an unprecedented rhombitruncated cuboctahedral arrangement of hexagonal columns that, to the best of our knowledges, was not yet encountered in biology or synthetic chemistry. We feel that the amphiphilic Janus dendrimer concept reported here is general and can be employed to discover other complex soft condensed matter morphologies.

2. Methods

2.1. Materials

Hydrochloric acid 12M (Fisher Chemical), *N*,*N*′-dicyclohexylcarbodiimide (DCC) (Chem-Impex), Pd on carbon 10% (Spectrum and TCI), pentaerythritol (Aldrich Chemical), benzaldehyde (Fisher Scientific), dimethylol propionic acid (Aldrich Chemical), and 2,2-dimethoxypropane (Acros Organics) were obtained from commercial sources and used without purification unless otherwise stated. CH_2Cl_2 (DCM) was dried over CaH_2 and freshly distilled before use.

2.2. Techniques

2.2.1. ^1H and ^{13}C NMR

^1H and ^{13}C NMR spectra were recorded at 500 and 126 MHz respectively, on a Bruker DRX (500 MHz) NMR spectrometer. All NMR spectra were measured at 23°C in $CDCl_3$. Chemical shifts (δ) are reported in ppm and coupling constants (J) are reported in Hertz (Hz). The resonance multiplicities in the ^1H NMR spectra are described as ‘s’ (singlet), ‘d’ (doublet), ‘t’ (triplet), ‘quint’ (quintet) and ‘m’ (multiplet) and broad resonances are indicated by ‘br’. Residual protic solvent of $CDCl_3$ (^1H, δ 7.26 ppm; ^{13}C, δ 77.16 ppm), and tetramethylsilane (TMS, δ 0 ppm) were used as the internal reference in the ^1H and ^{13}C NMR spectra. The absorptions are given in wavenumbers (cm^{-1}). NMR spectra were analysed and exported by TopSpin 4.07 (Bruker).

2.2.2. Thin-layer chromatography (TLC)

Evolution of the reaction was monitored by TLC using silica gel 60 F254 precoated plates (E. Merck) and individual compounds were visualised by UV light with a wavelength of 254 nm. Purifications by flash column chromatography was performed using flash silica gel from Silicycle (60 Å, 40–63 µm) with the indicated eluent.

2.2.3. High-pressure liquid chromatography (HPLC)

The purity of the compounds was determined by a combination of TLC and high-pressure liquid chromatography (HPLC) which was carried out using Shimadzu LC-20AD high-performance liquid chromatograph pump, a PE Nelson Analytical 900 Series integration data station, a Shimadzu SPD-10A VP (UV-vis, $\lambda = 254$ nm) and three AM gel columns (a guard column, two 500 Å, 10 mm columns). THF was used as solvent at the oven temperature of 23°C. Detection was done by UV absorbance at 254 nm.

2.2.4. Matrix assisted laser desorption ionization-time of flight (MALDI-TOF) mass spectrometry

MALDI-TOF mass spectrometry was performed on a PerSeptive Biosystem-Voyager-DE (Framingham, MA) mass spectrometer equipped with nitrogen laser (337 nm) and operating in linear mode. Internal calibration was performed using Angiotensin II and Bombesin as standards. The analytical sample was obtained by mixing the THF solution of the sample (5–10 mg/mL) and THF solution of the matrix (2,5-dihydroxybenzoic acid, 10 mg/mL) in a 1/5 (v/v) ratio. The prepared solution of the sample and the matrix (0.5 µL) was loaded on the MALDI plate and allowed to dry at 23°C before the plate was inserted into the vacuum chamber of the MALDI instrument. The laser steps and voltages applied were adjusted depending on both the molecular weight and the nature of each analysed compound.

2.2.5. Differential Scanning Calorimetry (DSC)

Transition temperatures and their associated enthalpy changes were determined with a Q100 differential scanning calorimeter from TA Instruments. Indium was used as the calibration standard at indicating heating and cooling rates. An Olympus BX51 optical microscope (100× magnification) equipped with a Mettler FP82HT hot stage and a Mettler Toledo FP90 Central Processor was used to verify thermal transitions. Melting points of samples were measured by an uni-melt capillary (Arthur H. Thomas Company) melting point apparatus prior to the DSC measurements.

2.2.6. Density measurements

The density (ρ) of aligned fibers was measured via Archimedes' Principle. Deionised water and methanol were selected as the two solvents to generate a combination of densities mixture solutions due to the insolubility of the samples (3,4,5)12G1-PE-BMPA-G1-$(OH)_4$ (**11**) in these solvents. A small piece of the fiber sample ($\sim$0.4 mg) was added in a scintillation vial filled with water. The fiber sample was found floating on the water in our first trial, indicating the density of the sample is less than 1.00 g/cm^3. In the second trial, a small piece of fiber sample was found sunk in pure methanol, indicating the density of our sample is higher than 0.792 g/cm^3. Deionised water was added dropwise to slightly increase the density of the solution until the fiber sample was suspended in the middle of the solution for at least 20 min. Upon equilibrium between the suspended sample fiber and the mixture solution, the density of the fiber is identical to that of the solution. The density of the solution was measured and calculated by using a calibrated pipette (1.000 mL, Rainin Classic™ manual single-channel pipette, 100–1000 μL) with a Mettler Toledo AB135-S/FACT balance (±0.01 mg accuracy) for three times. The density of **11** was calculated to be 0.891 g/cm^3 (average of three measurements).

2.2.7. Fiber preparation for X-ray diffraction (XRD) experiments

Dried samples purified by column chromatography or by recrystallization were loaded into the sample chamber of a custom-made extrusion device [74]. The fiber was heated to 40°C, extruded and then cooled to 23°C. In general, the thickness of an aligned samples is around 0.3–0.7 mm, and the length of the fiber is around 3–7 mm. Subsequently, the aligned fiber was sealed in a glass capillary that was used for XRD measurements.

2.2.8. X-ray diffraction (XRD) measurements

XRD experiments were performed using the Dual-source and Environmental X-ray Scattering (DEXS) system. Measurements were conducted using Cu-Kα1 radiation ($\lambda = 1.542$ Å) on a Xeuss 2.0 instrument with the slits of 1.2 × 1.2 mm for high flux. To minimised attenuation and background scattering, internal vacuum was maintained along the length of the flight tube, and within the sample chamber. Temperature control of the fiber samples was achieved by using a Linkam apparatus. Data collected from eight detectors were combined and integrated in the final XRD pattern. Fiber samples were held in glass capillaries (Charles Supper Company) (1.0 mm in diameter), placed in a temperature-controlled oven (temperature precision: ±0.1°C, temperature range: from -10 to 210°C). All XRD measurements were conducted with the aligned sample axis perpendicular to the beam direction. The sample-to-detector distance was 571 mm. Primary XRD structural analysis was performed using Datasqueeze (version 3.0.5).

3. Results and discussion

3.1. A brief introduction to the principles of self-organisation of self-assembling dendrons, dendrimers and dendronized polymers

A brief summary of the principles of self-organisation of self-assembling dendrons, dendrimers and dendronized polymers is outlined in Figure 1. Self-assembling dendrons, dendrimers and dendronized polymers produce a large diversity of supramolecular architectures that self-organize into periodic and quasiperiodic arrays. The two most important supramolecular architectures for this discussion are helical columns [16,17,74–94] and helical spheres [95–99]. The self-assembling dendron or dendrimer conformations that are relevant for this manuscript are taper, conical and crown [16,17,74,76]. The tapered and conical conformers are under a certain set of conditions interconvertible and therefore, were classified by us as being quasi-equivalent [9,18,101,102]. The quasi-equivalent concept was transplanted from the quasi-equivalent proteins that change their shape during the self-assembly of icosahedral viruses [103]. The crown conformation can be inverted and display a transient disk-like conformation during this process [95,96]. Both conical and crown conformers self-assemble into helical supramolecular spheres and during crown-inversion and conical-taper interchange they transform helical spheres

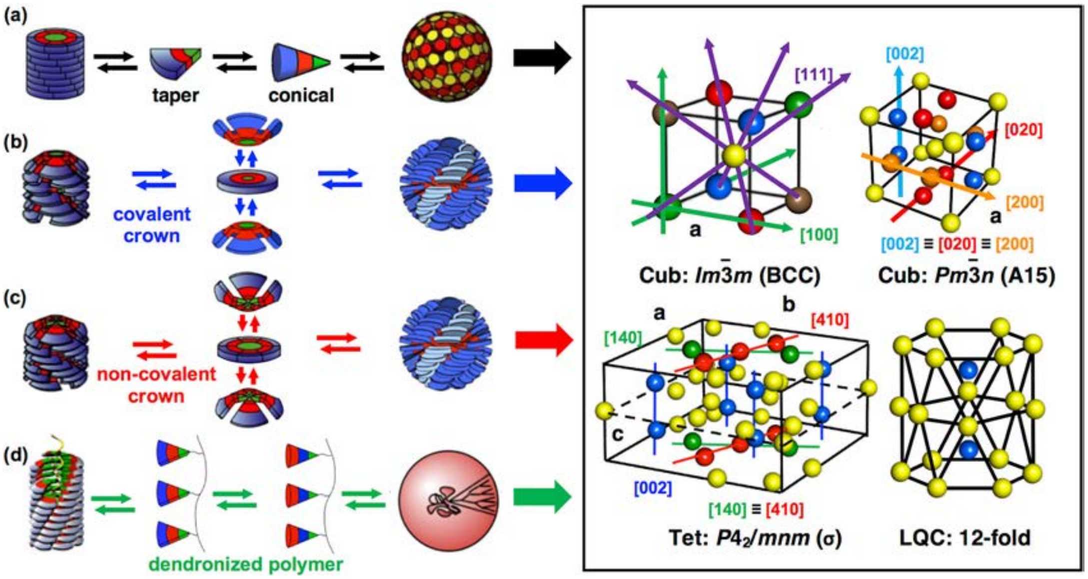

Figure 1. Mechanisms of transitions between columnar phases and cubic phases with taper (a), covalent crown (b), non-covalent crown (c) and dendronized polymer (d) as self-assembling dendrons.

into helical columns. The reverse process is also valid. All helical columns self-organize into columnar hexagonal arrays while helical spheres self-organize BCC and A15 cubic, tetragonal or σ F-K and 12-fold liquid quasicrystal (LQC) phases.

The mechanism of transformation of a supramolecular column into supramolecular spheres is illustrated in Figure 2. Figure 2a shows how intracolumnar motion moves molecules to create lower and higher electron densities. Ultimately the column splits into spheres. The reverse process is also accessible. Conical to tapered dendron-dendron conformations mediate this process. However, the most efficient column to sphere and sphere to column transition is mediated by crown inversion since this represents a concerted one step process [65]. Conical to tapered sphere to column and column to sphere transition is not accompanied by any memory or epitaxial orientation memory effect [16–31,100–102]. However, in the case of supramolecular spheres and columns assembled from

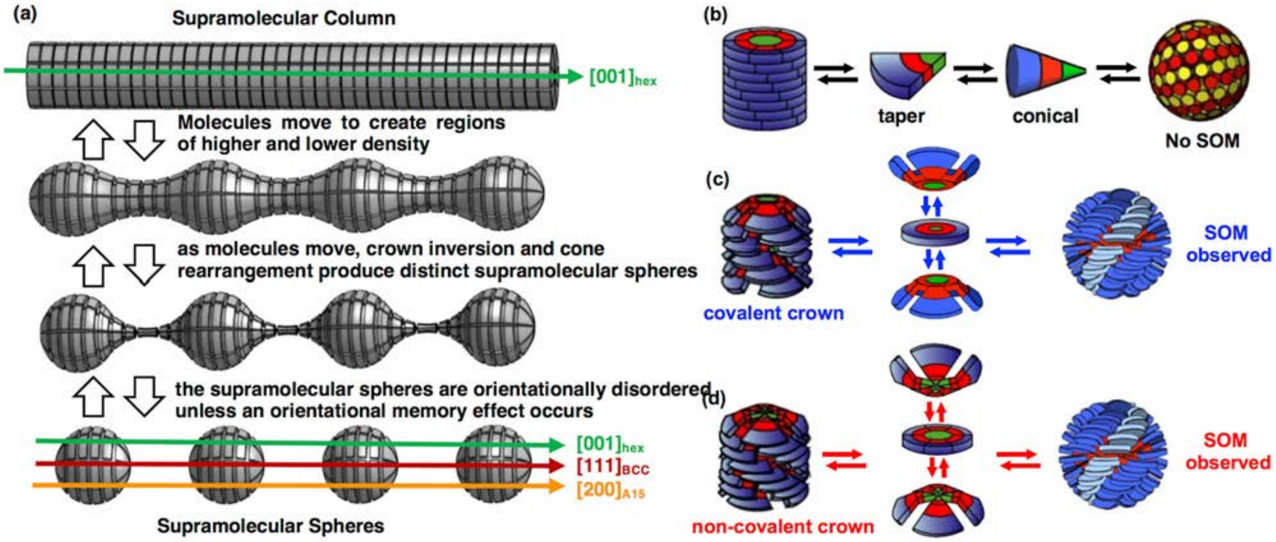

Figure 2. Mechanisms of reversible transformation between supramolecular columns and spheres. Supramolecular hexagonal columns assembled from tapers (b), covalent crowns (c) and non-covalent crowns (d) transform into supramolecular spheres. SOMs were observed *via* covalent crown and non-covalent crown mechanisms.

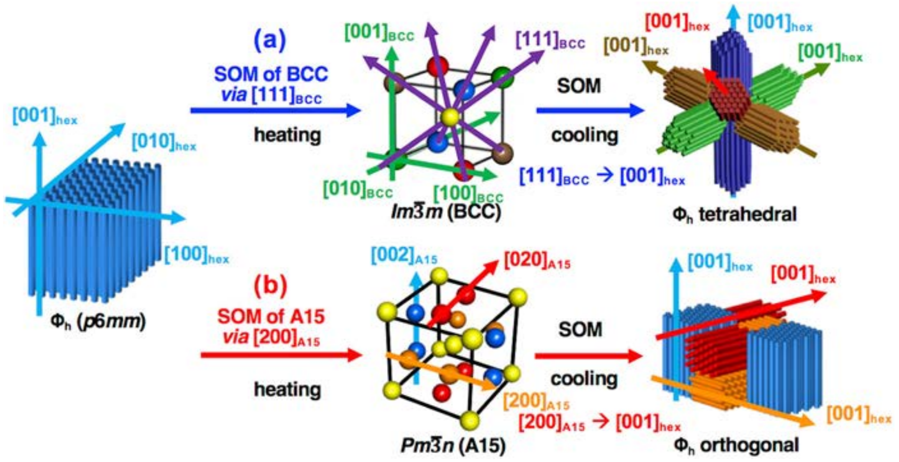

Figure 3. Summary of already published SOMs generating new hexagonal arrangements of columns. (a) Tetrahedral arrangement by following the close contact direction along $[111]_{\text{BCC}} \rightarrow [001]_{\text{hex}}$ in $Im\bar{3}m$ (BCC). (b) Orthogonal arrangement by following the close contact direction along $[200]_{\text{A15}} \rightarrow [001]_{\text{hex}}$ in $Pm\bar{3}n$ (A15). Covalent crowns are forming columns and spheres in (a) and (b) while supramolecular H-bonding crown-assembled columns and spheres do not follow these mechanisms.

crown conformations a SOM effect was discovered [62,63,65].

So far this was quantified for the case of the transition from columnar hexagonal to BCC [63] and back and from columnar hexagonal to A15 [62,65] and back. Figure 3 illustrates these SOM processes. In the case of the BCC phase, the spheres from the $[111]_{\text{BCC}}$ directions are in closer contact than all other directions of spheres. Therefore, when columns are assembled from crowns the SOM process from columnar hexagonal to BCC and back to columnar hexagonal occurs and generates a tetrahedral arrangement of columnar hexagonal columns that were nucleated by the close contact spheres from the BCC lattice (Figure 1a) [63]. In the case of A15 phase the spheres along the $[200]_{\text{A15}}$, $[020]_{\text{A15}}$ and $[002]_{\text{A15}}$ directions are in closer contact than all other spheres [62]. Alternatively, an orthogonal arrangement of hexagonal columns is generated by SOM at the transition from columnar hexagonal to A15 and back to columnar hexagonal (Figure 1b) [62]. In both cases the crowns were covalently linked. When the crown was linked by H-bonding rather than covalent bonds, the supramolecular columns and spheres assembled from the supramolecular crown, selected a different sphere direction from that of the closest contact spheres [65], that may need to be revised in view of the results that will be presented here.

3.2. Synthesis of the (3,4,5)12G1-PE-BMA-G1-$(OH)_4$, 11, amphiphilic Janus dendrimer

The synthesis of the amphiphilic Janus dendrimer (3,4,5)12G1-PE-BMPA-G1-$(OH)_4$ (**11**) was briefly described previously [66,104]. An improved and optimised synthesis was in the meantime elaborated. This synthesis is outlined in Figure 4 and detailed in the Supplemental Information. Briefly, **1** was monoprotected with benzaldehyde under acidic conditions for 3h to produce **3** in 73% yield [66,105] after purification by recrystallization from toluene. **6** was prepared in 84% yield also in 2 h by acetal protection of the two OH groups of **4** with **5** under acid catalysed conditions in acetone at 23°C. The product **6** was extracted with DCM, the organic phase was washed with water, and the solvent was evaporated without additional purification [106]. **7** was prepared by a recently optimised method by alkylation of methyl 3,4,5-trihydroxybenzoate with *n*-dodecyl bromide in dimethyl formaldehyde with K_2CO_3 as base for 2 h at 120°C, followed by hydrolysis with KOH for 1 h in ethanol at 80°C and subsequent acidification [107]. Steglich esterification of **7** with **3** by DCC and 4-(dimethylamino)pyridinium 4-toluenesulfonate (DPTS) [108] in DCM at 23°C after 12 h produced **8** in 89% isolated yield after purification by silica gel column chromatography with hexane/ethyl acetate (20/1) as eluent [66]. Deprotection of **8** to produce **9** in 99% yield was carried out by hydrogenolysis catalysed with Pd/C without further purification [66]. Esterification of **9** with **6** produced **10** in 86% yield after purification by silica gel column chromatography with hexane/ethyl acetate (5/1) as eluent. Compound **10** was then deprotected by aqueous hydrochloride acid in a mixture of methanol and DCM for 12h to generate **11**. Compound **11** was isolated by silica gel column chromatography with hexane/ethyl acetate (1/2) as eluent and recrystallization from methanol to obtain white crystal in 86% yield and 100% purity as demonstrated

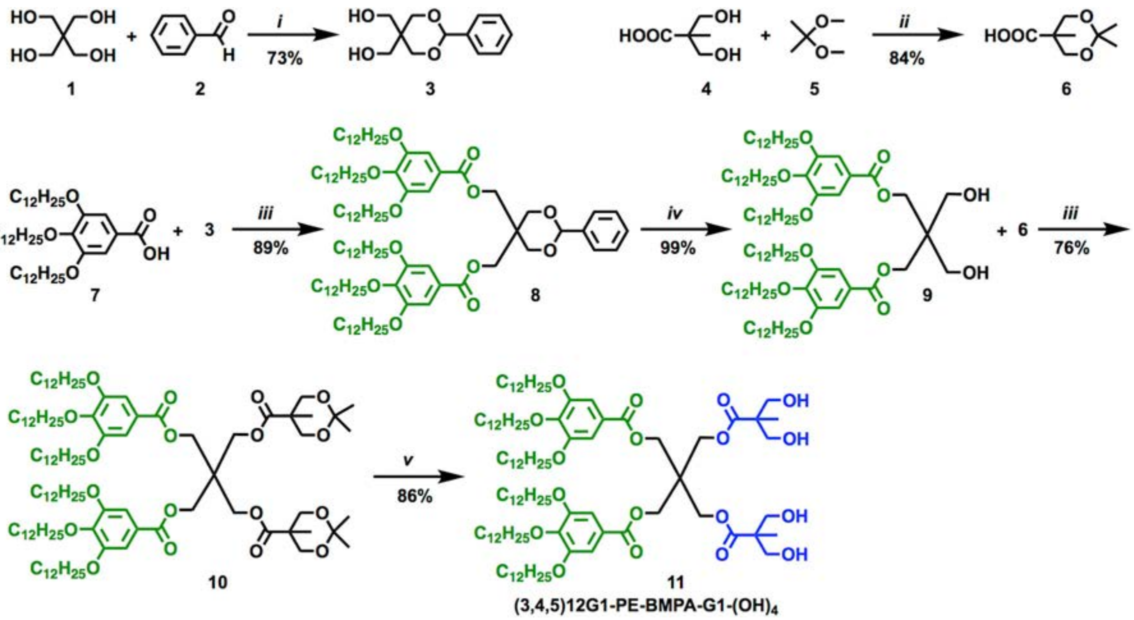

Figure 4. Synthesis of amphiphilic Janus dendrimer **(3,4,5)12G1-PE-BMPA-G1-(OH)$_4$ (11)**. Reagents and conditions: (i) HCl (aq.), H_2O, 25°C, 3 h; (ii) TsOH·H_2O, acetone, 23°C, 2 h; (iii) DCC, DPTS, DCM, 23°C, 12 h; (iv) H_2, Pd/C, DCM, MeOH, 23°C, 12 h; (v) HCl (2M), MeOH, DCM, 23°C, 12 h.

by NMR, HPLC and MALDI-TOF analysis (SI, Figure S1–S3) [66,104].

3.3. Thermal and structural analysis of assemblies generated from 11 by differential scanning calorimetry and oriented fiber X-ray diffraction

Thermal analysis of **11** (Figure 5a) was performed by differential scanning calorimetry (DSC) at 10°C/min. All phases were identified by X-ray diffraction (XRD). Assemblies of **11**, as resulted from its synthesis, exhibited three first-order transitions (Figure 5b, Figure S4 and Table 1) on the heating and cooling scans. On heating, **11** assemblies show two columnar hexagonal crystal (Φ_h^k) phases, a $Pm\bar{3}n$ cubic phase, also known as the F-K A15 phase, and an isotropic liquid phase. On cooling, in addition to the A15 and columnal hexagonal crystal phase a monotropic columnar hexagonal liquid crystal phase is also observed. Indexing of all phases, except for the monotropic columnar hexagonal liquid crystal phase, and calculation of lattice parameters was performed by using Small-Angle X-ray Scattering (SAXS) (Figure 5c, e, f, g, i, j). Wide-Angle X-ray Scattering (WAXS) was performed to index the intermolecular distance along the fiber axis in the Φ_h^k phase that is 4.2 Å (Figure 5d, h). The off-meridional features of the WAXS patterns indicated that the columnar hexagonal phase was helical and crystalline. The details and the models of the helical columns will be discussed later. Three $(100)_{\mathrm{hex}}$, $(110)_{\mathrm{hex}}$ and $(200)_{\mathrm{hex}}$ peaks with the ratio of the q values of $1{:}\sqrt{3}{:}2$ on the equator in the Φ_h^k at 30°C (Figure 5c, g) confirm that the fiber sample was well-aligned prior to the heating and cooling X-ray analysis cycles. Upon heating to 70°C, oriented peaks of $(200)_{\mathrm{A15}}$, $(210)_{\mathrm{A15}}$ and $(211)_{\mathrm{A15}}$ with the ratio of the q values equal to $\sqrt{4}{:}\sqrt{5}{:}\sqrt{6}$ demonstrated the formation of the $Pm\bar{3}n$ cubic or A15 F-K phase (Figure 5e, i).

Upon cooling from the $Pm\bar{3}n$ cubic phase at 70°C to the columnar hexagonal (Φ_{h}) liquid crystal phase at 20°C, six sharp $(100)_{\mathrm{hex}}$ features were observed in the X-ray fiber diffractogram of Φ_{h} (Figures 5e and 6) phase. However, due to its monotropic nature, no WAXS could be recorded for the columnar hexagonal liquid crystal phase at this time. These features are consistent with the combined orientations of $(210)_{\mathrm{A15}}$ and $(211)_{\mathrm{A15}}$ observed in the $Pm\bar{3}n$ cubic phase which account for the supramolecular orientational memory (SOM). As shown more clearly in the azimuthal plot, the orientations of $(100)_{\mathrm{hex}}$ are preserved from $[421]_{\mathrm{A15}}$ (Figure 6).

The SOM from $Pm\bar{3}n$ to columnar hexagonal (Φ_{h}) phase observed from non-covalent supramolecular crown is different from the SOM observed from covalent crowns assemblies [62,63,65]. As already reported [62], covalent crown assemblies generate an orthogonal arrangement of hexagonal columns (Figure 3b). When covalent crown assemblies are replaced with supramolecular non-covalent crown-based assembles, a rhombitruncated cuboctahedral arrangement of hexagonal columns, to be discussed later, was discovered.

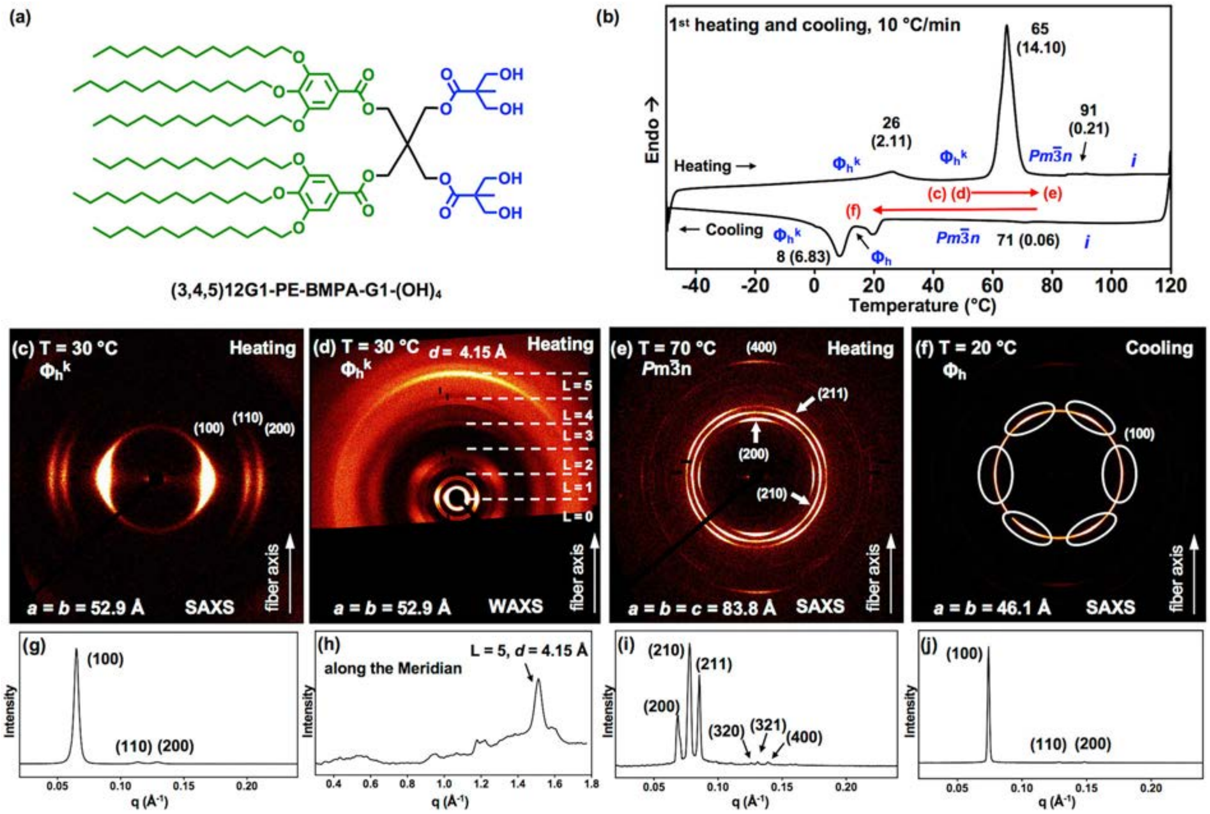

Figure 5. Structural analysis of the supramolecular assemblies of **11** generated by SOM. (a) Structure of **11**. (b) DSC traces of first heating and cooling scans of **11** obtained at 10°C/min. Phases indexed by XRD, transition temperatures (in °C), and associated enthalpy changes (in parentheses in kcal/mol) are indicated. (c–f) XRD patterns during heating and cooling cycles of an aligned fiber sample prepared by extrusion. Lattice parameters, temperatures and peak assignments are shown. (g–j) XRD diffractograms with (*hkl*) indices indicated. For the *P*6*mm* hexagonal phases, (100), (110) and (200) are listed with the ratio of the *q* value equal to 1:$\sqrt{3}$:2. For the $Pm\bar{3}n$ cubic phase, (200), (210) and (211) are listed with the ratio of the *q* value of $\sqrt{4}$:$\sqrt{5}$:$\sqrt{6}$. Peaks assignments were indexed by using Datasqueeze software (version 3.0.5).

Table 1. Transition temperatures and associated enthalpy changes of (3,4,5)12G1-PE-BMPA-G1-(OH)$_4$ determined by DSC and phases determined by XRD.

	Phase transition (°C) and corresponding enthalpy changes (kcal/mol)[a]	
	First and second heating	First and second cooling
(3,4,5)12G1-PE-BMPA-G1-(OH)$_4$	$\boldsymbol{\Phi}_h{}^k$ 31 (1.25) Φ_h^k 66 (15.22) $\boldsymbol{Pm\bar{3}n}$ 91(0.21) $\boldsymbol{i}$ Φ_h^k 20 (4.13) $\boldsymbol{\Phi_h}$ 65 (11.90) $\boldsymbol{Pm\bar{3}n}$	$\boldsymbol{i}$ 71(0.06) $\boldsymbol{Pm\bar{3}n}$ 20 Φ_h 11(−9.90) Φ_h^k $\boldsymbol{Pm\bar{3}n}$ 23 (−0.80) $\boldsymbol{\Phi_h}$ 11(−6.23) Φ_h^k

[a] $\boldsymbol{\Phi_h}$ – 2D columnar hexagonal phase; $\boldsymbol{Pm\bar{3}n}$ – cubic, F-K A15 phase; $\boldsymbol{i}$ – isotropic. Note: quantitative uncertainties are ±1 °C for thermal transition temperatures and ∼ 2% for the associated enthalpy changes. Heating and cooling rate: 10°C/min.

3.4. Structural and retrostructural analysis by oriented fiber XRD and molecular models of the supramolecular crowns in the Φ_h^k and A15 phases

To generate a non-covalent supramolecular crown from the Janus dendrimer **11** with three molecules per 4.2 Å stratum, μ equal to 3 (Table 2), multiple inter- and intramolecular H-bonds as shown in Figure 7 must occur.

It is important to mention that previously [65], no SOM was observed when there were only two alcohol groups per stratum, derived from one -OH per molecule, interacting *via* H-bonding at the apex of the self-assembling dendrons. When the number of the alcohol groups at the apex increased to 12 per stratum, derived from 3 molecules each containing four -OH, as in the case of **11** (Figure 8c), most probably as it will be discussed later a dynamic non-covalent crown was formed. This supramolecular crown mediated the formation of the new SOM reported here. A comparison of all molecules exhibiting SOM reported in our previous publications [62,63,65] is summarised in Table 2. For molecules that adopt the conformation of covalent crowns, for example, PBI, CTV and CTTV, supramolecular spheres are formed with a relatively low number of molecules (μ = 7 or 12). For the molecules

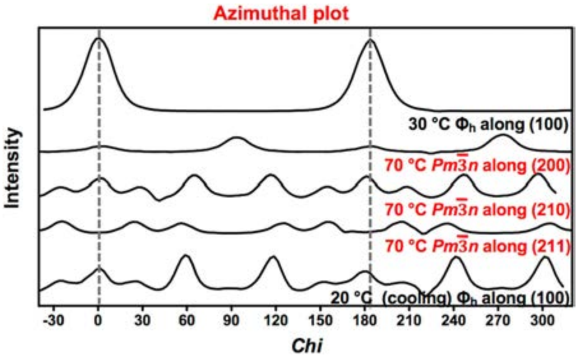

Figure 6. Azimuthal plots from XRD patterns of **11** with temperatures and phases along $(100)_{hex}$, $(200)_{A15}$, $(210)_{A15}$ and $(211)_{A15}$.

that form the dynamic non-covalent crowns, such as (4Pr-(3,4,5Pr)^2)-12G2-COOH [65] and most probably also **11**, supramolecular spheres are formed from a relatively larger number of molecules (μ = 24 or 30). These data demonstrate that increasing the number of H-bond interactions at the apex is a requirement for the generation of dynamic non-covalent crowns forming assemblies that exhibit SOM.

The structural and retrostructural analysis of the oriented fiber by SAXS and WAXS X-ray diffraction data from Figure 5 and Table 2, together with the experimental density of the fiber by conventional methods elaborated in our laboratory [16,17] including the helical diffraction theory [74,109] provided the two mechanisms of self-assembly of helical columns from the amphiphilic Janus dendrimer **11** illustrated in Figure 8.

Figure 8b shows a supramolecular 16_5-helix assembled by an H-bonded helical supramolecular polymer from the conformation of the dendron shown on top of the helical column from Figure 8b. Figures 8c and d show an alternative model for a triple 15_1-helix that is generated by the assembly of a supramolecular crown generated by H-bonding and shown on top of the helical column from Figure 8d. Crown inversion within the supramolecular helical column according to the mechanism from Figures 1 and 2 generated the supramolecular sphere shown in Figure 8e. The mechanism of transition from helical column to helical sphere illustrated in Figure 8c–e was already demonstrated to be responsible for the generation of SOM [62,63,65]. However, at this time we cannot conclude that the mechanism from Figure 8c,d is responsible for the SOM observed here. An alternative mechanism can also be envisioned. This alternative mechanism may occur by the inversion of the helical H-bonded supramolecular polymer column from Figure 8b into a supramolecular helical sphere. The major difference in between these two mechanisms is that breaking the H-bonding of the supramolecular helical polymer from Figure 8b,e is required in one case while no H-bond braking is required for the mechanism from Figure 8c–e. Therefore, the crown inversion mechanism seems to be more favourable. However, more structural and simulation work is required to discriminate between these two mechanisms and also for the generation of a model for the columnar structure of the columnar hexagonal liquid crystal phase that is expected to be closely related

Table 2. Structural analysis of crown-like conformation of self-assembling dendrons and dendrimers by small-angle XRD to search for the orientational memory effect.

Molecule	T (°C)	Phase^a	d_{100}, d_{110}, d_{200}, d_{210}, d_{300} (Å)^b d_{110}, d_{200}, d_{211} (Å)^c d_{200}, d_{210}, d_{211}, d_{320}, d_{321}, d_{400} (Å)^d	a, b, c (Å)^e	$D_{col}{}^f/D_{sph}{}^g$ (Å)	μ^h	SOM	Ref.
(3,4,5)12G1-PE-BMPA-G1-(OH)$_4$^{i}	70	$\boldsymbol{Pm\bar{3}n}$	42.1, 37.6, 34.4, 23.2, 22.4, 20.9^d	83.8, 83.8, 83.8	52.0^g	24	**Yes**	***this work***
	30	Φ_h^k	45.5, 26.3, 22.7, 17.2, 15.2^b	52.9, 52.9, –	52.9^g	3		
	20	$\mathbf{\Phi_h}$	39.9, 23.1, 19.9^b	46.1, 46.1, –	46.1^f	3		
(4Pr-(3,4,5Pr)^2)-12G2-COOH^i	60	$\boldsymbol{Pm\bar{3}n}$	53.4, 47.8, 43.6, –, –, –^{d}	106.9, 106.9, 106.9	66.3^g	30	**Yes**	65
	30	$\mathbf{\Phi_h}$	47.4, 27.2, 23.6^b	54.5, 54.5 –	54.5^f	2		
(3,4Pr-3,4,5)12G2-0-PBI	180	**BCC**	38.4, 25.9, 21.1^c	51.6, 51.6, 51.6	44.7^g	12	**Yes**	63
	80	Φ_h^{io}	42.9, –, 21.5^b	49.5, 49.5, –	49.5^f	2		
	0	Φ_h^k	42.5, 24.5, 21.2^b	48.8, 48.8, 19.2	48.8^f	2		
(3,4,5)12G1-CTV	80	$\boldsymbol{Pm\bar{3}n}$	36.6, 32.7, 29.8, –, –, –^{d}	73.5, 73.5, 73.5	45.6^g	7	**Yes**	62
	65	Φ_h^{io}	35.6, 20.5, 17.8^b	41.1, 41.1, –	41.1^f	1		
(4-3,4,5)12G1-CTTV	125	$\boldsymbol{Pm\bar{3}n}$	46.1, 41.2, 37.6, –, –, –^{d}	92.2, 92.2, 92.2	57.2^g	7	**Yes**	65
	25	Φ_h	43.4, 25.0, 21.7^b	50.1, 50.1, –	50.1^f	1		

[a] Phase notation: $\mathbf{\Phi_h}$ –columnar hexagonal liquid crystal phase; Φ_h^k – columnar hexagonal crystalline phase; **BCC** – body-centered cubic phase; $\boldsymbol{Pm\bar{3}n}$ –cubic phase.

[b] Experimental d-spacings for the $\mathbf{\Phi_h}$ phases.

[c] Experimental d-spacings for the **BCC** phase.

[d] Experimental d-spacings for the $\boldsymbol{Pm\bar{3}n}$ phase.

[e] Lattice parameters calculated using $d_{hk} = (\sqrt{3}a/2)\cdot(h^2 + k^2 + hk)^{-1/2}$ for hexagonal phases, and $d_{hkl} = (a)\cdot(h^2 + k^2 + l^2)^{-1/2}$ for the cubic phase.

[f] Column diameter for $\mathbf{\Phi_h}$ phases ($D_{col} = a$).

[g] Sphere diameter for the **BCC** phase ($D_{sphere} = \sqrt{3}a/2$); $D_{sph} = 2(3a^3/32\pi)^{1/3}$ for $\boldsymbol{Pm\bar{3}n}$ phase.

[h] Number of monodendrons per sphere in the cubic phase or stratum in the hexagonal phase.

[i] Supramolecular dynamic crowns.

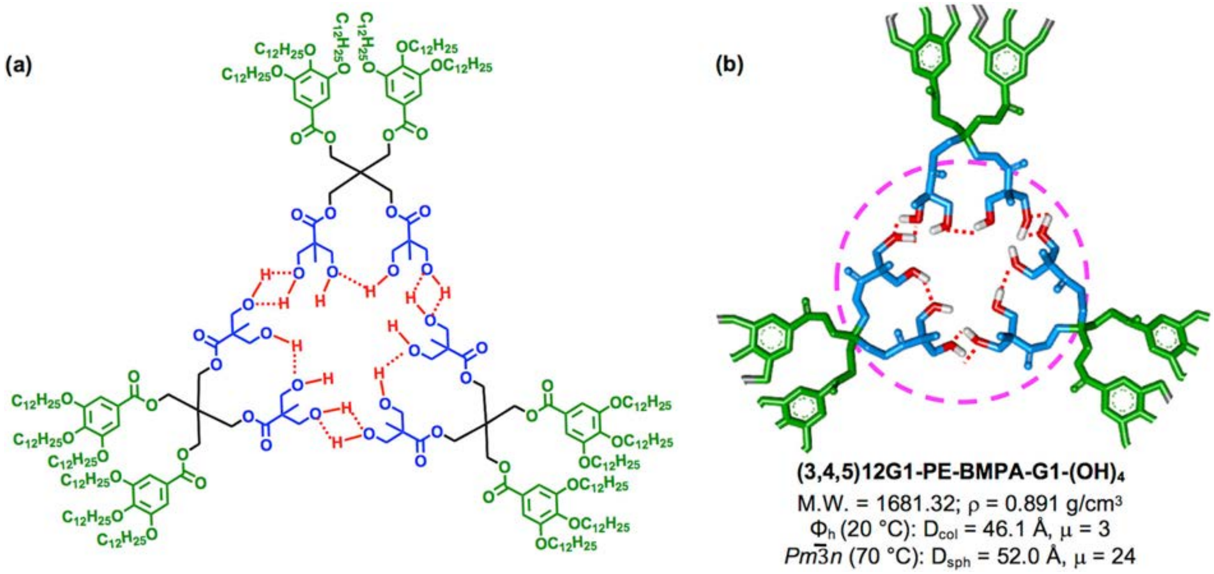

Figure 7. Chemical structure (a) and molecular models (b) with H-bonds at the apex for the formation of non-covalent crown from three self-assembling amphiphilic Janus dendrimer **11**.

to the column from the corresponding columnar hexagonal crystal phase. This research is in progress in our laboratory and will be reported in due time.

3.5. The mechanism of epitaxial nucleation responsible for the SOM effect

3D views of the transition from $Pm\bar{3}n$ to columnar hexagonal lattices are shown in Figure 9 with $(210)_{A15}$ (green) and $(112)_{A15}$ (orange) Miller planes illustrated in the cubic unit cell. Upon cooling from 70°C to 20°C, 5 supramolecular spheres at $z = 1/2$ move to be aligned in the $[421]_{A15}$ direction (Figure 9). Two supramolecular spheres at $z = 0, 1$ translate to $z = 1/8, 7/8$ (Figure 9) to generate the columnar hexagonal liquid crystal phase with a rhombitruncated cuboctahedral arrangement. The 421_{A15} vector is parallel to the $(\bar{1}20)_{A15}$, $(0\bar{1}2)_{A15}$ and $(1\bar{1}\bar{2})_{A15}$ planes and the Azimuthal plot of the $(100)_{hex}$ is the combination of the Azimuthal plots of the $(210)_{A15}$ and $(211)_{A15}$ (Figure 6). This mechanism allows minimum distortions of the lattice parameters in the columnar hexagonal phase.

3.6. The rhombitruncated cuboctahedral arrangement of hexagonal columns self-organised by SOM

There are three possible directions equivalent to [421] at the corner of the unit cell (yellow spheres) (Figure 10a upper). In addition, there are other three possible directions which are different but also equivalent to [421] that start from the body centre of the $Pm\bar{3}n$ unit cell (yellow sphere) (Figure 10a lower). Due to the symmetry of the cubic lattice, the number of directions equivalent to [421] is 8 times the 6 directions mentioned in Figure 9a, which represents 48 directions in total (Figure 10b, c). Figure 10b illustrates the 48 directions that hexagonal arrays of columns form *via* the SOM effect. These directions are generated with hexagonal arrays of columns as shown in Figure 10c. This arrangement corresponds to a rhombitruncated cuboctahedron, that to the best of our knowledge, although more primitive than biological assemblies created from proteins, was never encountered in biology or in synthetic supramolecular chemistry. Bundles of α-helical proteins are widely available in biology. They were discovered simultaneously and independently by Pauling and Corey [110] and by Crick [111] and are known as coiled-coil α-helix protein structures. Recently, a periodic table of coiled-coil proteins was elaborated [112]. Mimics of three and four-bundles of helical columns were elaborated by our laboratory *via* complex multistep synthetic methods [16,17,113–116]. However, the simplicity of the SOM method for the design of bundles of helical columns organised in unprecedentedly complex architectures such as tetrahedral [63], orthogonal [62], distorted dodecahedral [65] and now in rhombitruncated cuboctahedral arrangement of hexagonal columns as shown in the present report (Figure 11) seems to exceed even the ability of biology, although with a much lower level of perfection. We would like to stress again that in view of the results reported here, the distorted dodecahedral morphology [65] will have to be reinvestigated. This will be done and reported in a different publication. Elucidating the mechanism of the SOM concept and extending it

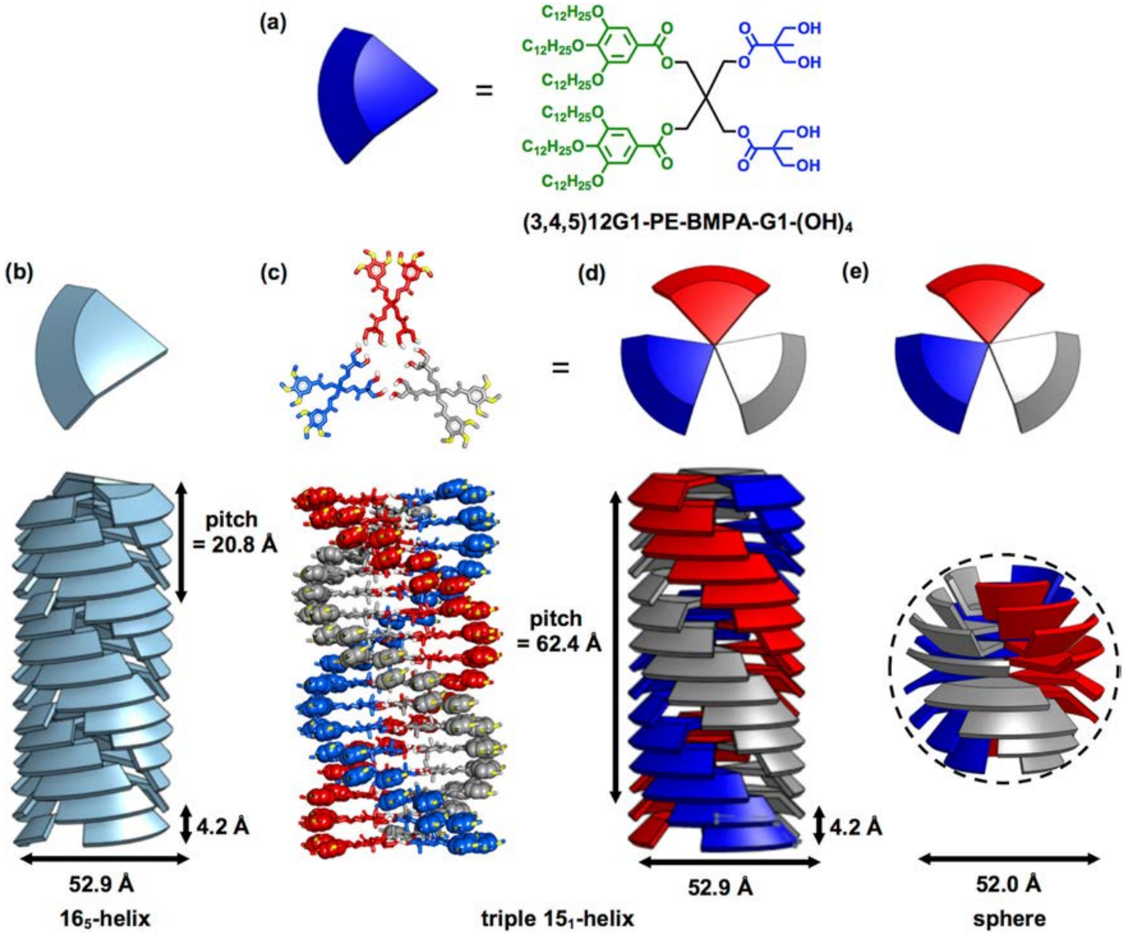

Figure 8. Structural and retrostructural analysis of the supramolecular assemblies of **11** (a) based on the SAXS data in Figure 5d and helical diffraction theory [74,109]. Schematic models of the two supramolecular helical columns self-organising the columnar hexagonal 2D and 3D lattices (b, c, d) and of the helical sphere (e) forming the *Pm*$\bar{3}$*n* lattice are shown. The two possible mechanisms, 16_5-helix ($\varphi = 360° \times 5/16 = 112.5°$, $c = 20.8$ Å $/16 = 1.3$ Å) generated when **11** jackets a helical H-bonded supramolecular polymer (b) and triple 15_1-helix ($\varphi = 360°/15 = 24°$, $c = 4.2$ Å $= 62.4$ Å $/15$) when **11** assembles into a supramolecular crown-trimer (c, d) forming the helical column are shown.

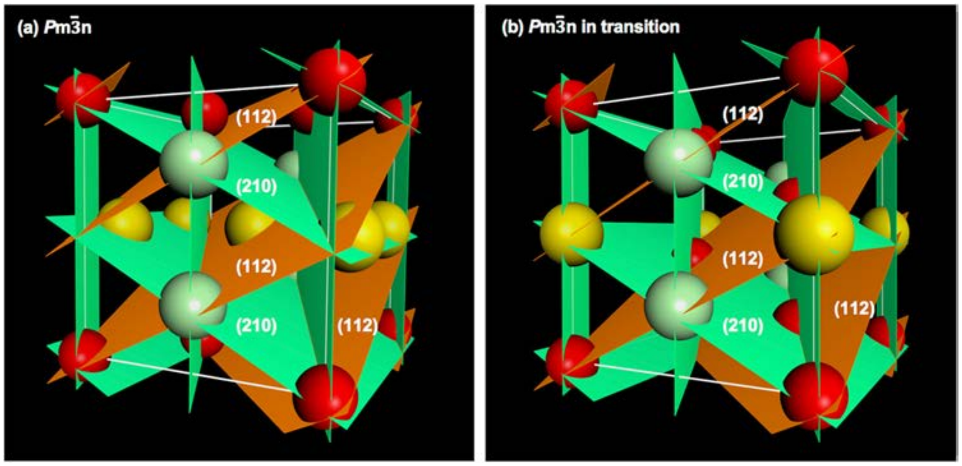

Figure 9. Two 3D views of the transition from *Pm*$\bar{3}$*n* to columnar hexagonal lattices with (210) and (112) Miller planes shown in the cubic unit cell. All the micelles are in the *Pm*$\bar{3}$*n* positions in (a). Micelles move to line up along the (421) direction of the unit cell in (b). The 421 vector is parallel to the ($\bar{1}$20), (0$\bar{1}$2) and (1$\bar{1}\bar{2}$) planes.

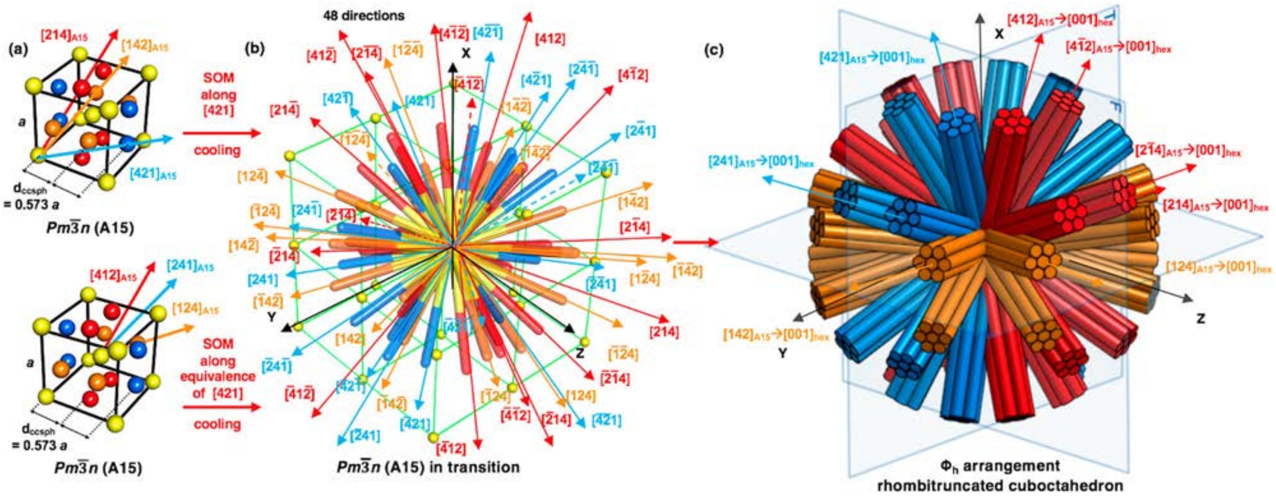

Figure 10. Modelling constructed according to structural and retrostructural analysis from XRD experiments. (a, b) Difference between close–contact distances along $[200]_{A15}$ and $[421]_{A15}$. Distance between two blue/red/orange sphere pairs is 0.5 a, which is 41.9 Å. Distances between the yellow sphere at the corner and the indicated blue/red/orange sphere are 0.573 a, which are 48.0 Å. The difference of the close–contact distances between $[200]_{A15}$ and $[421]_{A15}$ is 6.1 Å. (b) SOM Mechanism of **11** supramolecular assemblies generated along $[421]_{A15}$.

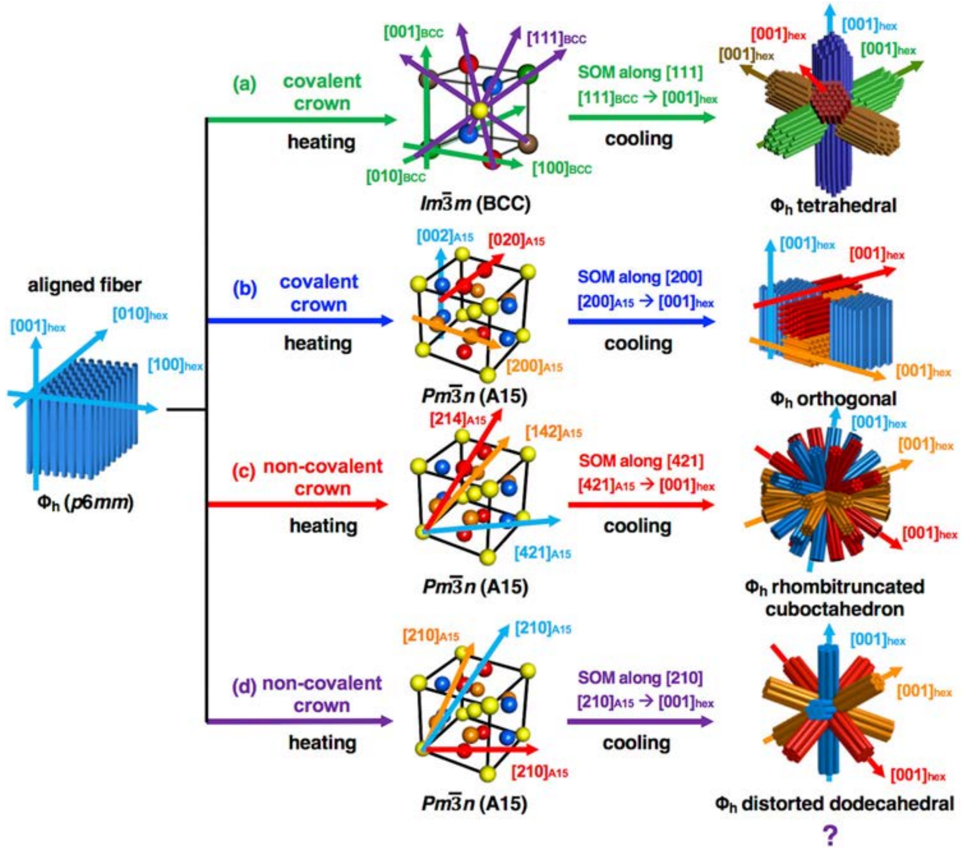

Figure 11. Summary of four SOMs generating tetrahedral, orthogonal, rhombitruncated cuboctahedral and distorted dodecahedral hexagonal arrangements of hexagonal columns. Upon heating and cooling, supramolecular helical columns and spheres assemblies undergo SOM with the close contact direction along $[200]_{A15} \rightarrow [001]_{hex}$ or $[111]_{BCC} \rightarrow [001]_{hex}$ while supramolecular assemblies consisted of non-covalent crowns undergo SOM with close-contact direction $[421]_{A15} \rightarrow [001]_{hex}$.

to other F-K phases will provide access, most probably, to even more complex architectures.

4. Conclusion

Amphiphilic Janus dendrimers known to self-assemble in water into biological membrane mimics named dendrimersomes and glycodendrimersomes were reported here to self-organize in bulk into 2D and 3D helical columnar hexagonal periodic arrays and helical spheres forming the A15 Frank Casper phase. This provides a new class of self-assembling molecules that self-organize Frank Casper phases and thus expands the diversity of organic compounds exhibiting these phases. In addition, the assemblies of the amphiphilic Janus dendrimer investigated here display also a supramolecular orientational memory (SOM) effect. The SOM effect observed here is epitaxially nucleated along the $[421]_{A15} \rightarrow [001]_{hex}$ close contact spheres self-organising an unprecedented rhombitruncated cuboctahedrom arrangement of helical hexagonal columns. The SOM effect indicates that the supramolecular columns of the low temperature hexagonal phase grow symmetrically along the equivalent directions $[421]_{A15}$ of the high temperature A15 cubic phase, while preserving the initial orientation as preferred axis (Figure 5c–f). The rhombitruncated cuboctahedral arrangement of hexagonal columns is related to the different possible orientations of the $[001]_{hex}$ axis of the domains of the hexagonal columnar phase on cooling, that the 48 unit vectors would each point to one of the vertices of a rhombitruncated cuboctahedral, the centre of which is placed at the origin. Different arrangements of columns including tetrahedral [63], orthogonal [62], distorted dodecahedral [65], and rhombitruncated cuboctahedral stem from the symmetrically equivalent epitaxial relations. Although the equilibrium phase of the columns should be a single crystal of columns with one orientation, the structure reported here is made of multidomains of hexagonal arrangement of columns. A mechanism for this self-organisation was proposed.

Disclosure statement

No potential conflict of interest was reported by the authors.

Funding

This work was supported by National Science Foundation; Division of Materials Research [grant numbers DMR-1720530 and DMR-1807127] the P. Roy Vagelos Chair at the University of Pennsylvania, and the Alexander von Humboldt Foundation (all to V.P.).

ORCID

Ning Huang http://orcid.org/0000-0001-8874-3439
Qi Xiao http://orcid.org/0000-0002-6470-0407
Mihai Peterca http://orcid.org/0000-0002-7247-4008
Xiangbing Zeng http://orcid.org/0000-0003-4896-8080
Virgil Percec http://orcid.org/0000-0001-5926-0489

References

[1] F.C. Frank and J.S. Kasper, Acta. Cryst. **11**, 184 (1958). doi:10.1107/S0365110X58000487
[2] F.C. Frank and J.S. Kasper, Acta. Cryst. **12**, 483 (1959). doi:10.1107/S0365110X59001499
[3] A.K. Sinha, Prog. Mater. Sci. **15**, 81 (1972). doi:10.1016/0079-6425(72)90002-3
[4] G. Ungar and X. Zeng, Soft Matter. **1**, 95 (2005). doi:10.1039/b502443a
[5] X. Zeng, G. Ungar, Y. Liu, V. Percec, A.E. Dulcey and J.K. Hobbs, Nature. **428**, 157 (2004). doi:10.1038/nature02368
[6] C.R. Iacovella, A.S. Keys and S.C. Glotzer, Proc. Natl. Acad. Sci. U.S.A. **108**, 20935 (2011). doi:10.1073/pnas.1019763108
[7] G. Ungar, V. Percec, X. Zeng and P. Leowanawat, Isr. J. Chem. **51**, 1206 (2011). doi:10.1002/ijch.201100151
[8] V.S.K. Balagurusamy, G. Ungar, V. Percec and G. Johansson, J. Am. Chem. Soc. **119**, 1539 (1997). doi:10.1021/ja963295i
[9] D.J.P. Yeardley, G. Ungar, V. Percec, M.N. Holerca and G. Johansson, J. Am. Chem. Soc. **122**, 1684 (2000). doi:10.1021/ja993915q
[10] D.R. Dukeson, G. Ungar, V.S.K. Balagurusamy, V. Percec, G.A. Johansson and M. Glodde, J. Am. Chem. Soc. **125**, 15974 (2003). doi:10.1021/ja037380j
[11] G. Ungar, Y. Liu, X. Zeng, V. Percec and W.-D. Cho, Science. **299**, 1208 (2003). doi:10.1126/science.1078849
[12] S.D. Hudson, H.-T. Jung, V. Percec, W.-D. Cho, G. Johansson, G. Ungar and V.S.K. Balagurusamy, Science. **278**, 449 (1997). doi:10.1126/science.278.5337.449
[13] A. Rapp, I. Schnell, D. Sebastiani, S.P. Brown, V. Percec and H.W. Spiess, J. Am. Chem. Soc. **125**, 13284 (2003). doi:10.1021/ja035127d
[14] P. Ziherl and R.D. Kamien, J. Phys. Chem. B. **105**, 10147 (2001). doi:10.1021/jp010944q
[15] Y. Li, S.-T. Lin and W.A. Goddard, J. Am. Chem. Soc. **126**, 1872 (2004). doi:10.1021/ja038617e
[16] B.M. Rosen, C.J. Wilson, D.A. Wilson, M. Peterca, M.R. Imam and V. Percec, Chem. Rev. **109**, 6275 (2009). doi:10.1021/cr900157q
[17] H.-J. Sun, S. Zhang and V. Percec, Chem. Soc. Rev. **44**, 3900 (2015). doi:10.1039/C4CS00249K
[18] V. Percec, C.-H. Ahn, G. Ungar, D.J.P. Yeardley, M. Möller and S.S. Sheiko, Nature. **391**, 161 (1998). doi:10.1038/34384
[19] V. Percec, W.-D. Cho, M. Möller, S.A. Prokhorova, G. Ungar and D.J.P. Yeardley, J. Am. Chem. Soc. **122**, 4249 (2000). doi:10.1021/ja9943400
[20] G. Ungar, V. Percec, M.N. Holerca, G. Johansson and J.A. Heck, Chem. Eur. J. **6**, 1258 (2000). doi:10.1002/(SICI)1521-3765(20000403)6:7 < 1258::AID-CHEM1258 > 3.0.CO;2-O

[21] V. Percec, W.-D. Cho, G. Ungar and D.J.P. Yeardley, J. Am. Chem. Soc. **123**, 1302 (2001). doi:10.1021/ja0037771

[22] V. Percec, C.M. Mitchell, W.-D. Cho, S. Uchida, M. Glodde, G. Ungar, X. Zeng, Y. Liu, V.S.K. Balagurusamy and P.A. Heiney, J. Am. Chem. Soc. **126**, 6078 (2004). doi:10.1021/ja049846j

[23] V. Percec, M. Peterca, M.J. Sienkowska, M.A. Ilies, E. Aqad, J. Smidrkal and P.A. Heiney, J. Am. Chem. Soc. **128**, 3324 (2006). doi:10.1021/ja060062a

[24] V. Percec, M.N. Holerca, S. Nummelin, J.J. Morrison, M. Glodde, J. Smidrkal, M. Peterca, B.M. Rosen, S. Uchida, V.S.K. Balagurusamy, M.J. Sienkowska and P.A. Heiney, Chem. Eur. J. **12**, 6216 (2006). doi:10.1002/chem.200600178

[25] V. Percec, B.C. Won, M. Peterca and P.A. Heiney, J. Am. Chem. Soc. **129**, 11265 (2007). doi:10.1021/ja073714j

[26] V. Percec, M. Peterca, A.E. Dulcey, M.R. Imam, S.D. Hudson, S. Nummelin, P. Adelman and P.A. Heiney, J. Am. Chem. Soc. **130**, 13079 (2008). doi:10.1021/ja8034703

[27] V. Percec, M. Peterca, Y. Tsuda, B.M. Rosen, S. Uchida, M.R. Imam, G. Ungar and P.A. Heiney, Chem. Eur. J. **15**, 8994 (2009). doi:10.1002/chem.200901324

[28] B.M. Rosen, D.A. Wilson, C.J. Wilson, M. Peterca, B.C. Won, C. Huang, L.R. Lipski, X. Zeng, G. Ungar, P.A. Heiney and V. Percec, J. Am. Chem. Soc. **131**, 17500 (2009). doi:10.1021/ja907882n

[29] M.N. Holerca, D. Sahoo, M. Peterca, B.E. Partridge, P.A. Heiney and V. Percec, Macromolecules. **50**, 375 (2017). doi:10.1021/acs.macromol.6b02298

[30] M.N. Holerca, D. Sahoo, B.E. Partridge, M. Peterca, X. Zeng, G. Ungar and V. Percec, J. Am. Chem. Soc. **140**, 16941 (2018). doi:10.1021/jacs.8b11103

[31] B.M. Rosen, M. Peterca, C. Huang, X. Zeng, G. Ungar and V. Percec, Angew. Chem. Int. Ed. **49**, 7002 (2010). doi:10.1002/anie.201002514

[32] S. Lee, M.J. Bluemle and F.S. Bates, Science. **330**, 349 (2010). doi:10.1126/science.1195552

[33] T.M. Gillard, S. Lee and F.S. Bates, Proc. Natl. Acad. Sci. U.S.A. **113**, 5167 (2016). doi:10.1073/pnas.1601692113

[34] K. Kim, M.W. Schulze, A. Arora, R.M. Lewis, M.A. Hillmyer, K.D. Dorfman and F.S. Bates, Science. **356**, 520 (2017). doi:10.1126/science.aam7212

[35] G.K. Cheong, F.S. Bates and K.D. Dorfman, Proc. Natl. Acad. Sci. U. S. A. **117**, 16764 (2020). doi:10.1073/pnas.2006079117

[36] D.V. Perroni and M.K. Mahanthappa, Soft Matter. **9**, 7919 (2013). doi:10.1039/c3sm51238j

[37] S.A. Kim, K.-J. Jeong, A. Yethiraj and M.K. Mahanthappa, Proc. Natl. Acad. Sci. U. S. A. **114**, 4072 (2017). doi:10.1073/pnas.1701608114

[38] C.M. Baez-Cotto and M.K. Mahanthappa, ACS Nano. **12**, 3226 (2018). doi:10.1021/acsnano.7b07475

[39] A. Jayaraman, D.Y. Zhang, B.L. Dewing and M.K. Mahanthappa, ACS Cent. Sci. **5**, 619 (2019). doi:10.1021/acscentsci.8b00903

[40] M. Huang, C.-H. Hsu, J. Wang, S. Mei, X. Dong, Y. Li, M. Li, H. Liu, W. Zhang, T. Aida, W.-B. Zhang, K. Yue and S.Z.D. Cheng, Science. **348**, 424 (2015). doi:10.1126/science.aaa2421

[41] K. Yue, M. Huang, R.L. Marson, J. He, J. Huang, Z. Zhou, J. Wang, C. Liu, X. Yan, K. Wu, Z. Guo, H. Liu, W. Zhang, P. Ni, C. Wesdemiotis, W.-B. Zhang, S.C. Glotzer and S.Z.D. Cheng, Proc. Natl. Acad. Sci. U.S.A. **113**, 14195 (2016). doi:10.1073/pnas.1609422113

[42] X. Feng, R. Zhang, Y. Li, Y. Hong, D. Guo, K. Lang, K.-Y. Wu, M. Huang, J. Mao, C. Wesdemiotis, Y. Nishiyama, W. Zhang, W. Zhang, T. Miyoshi, T. Li and S.Z.D. Cheng, ACS Cent. Sci. **3**, 860 (2017). doi:10.1021/acscentsci.7b00188

[43] Z. Su, C.-H. Hsu, Z. Gong, X. Feng, J. Huang, R. Zhang, Y. Wang, J. Mao, C. Wesdemiotis, T. Li, S. Seifert, W. Zhang, T. Aida, M. Huang and S.Z.D. Cheng, Nature Chem. **11**, 899 (2019). doi:10.1038/s41557-019-0330-x

[44] Y. Liu, T. Liu, X. Yan, Q.-Y. Guo, J. Wang, R. Zhang, S. Zhang, Z. Su, J. Huang, G.-X. Liu, W. Zhang, W. Zhang, T. Aida, K. Yue, M. Huang and S.Z.D. Cheng, Giant. **4**, 100031 (2020). doi:10.1016/j.giant.2020.100031

[45] P. Mariani, V. Luzzati and H. Delacroix, J. Mol. Biol. **204**, 165 (1988). doi:10.1016/0022-2836(88)90607-9

[46] R. Vargas, P. Mariani, A. Gulik and V. Luzzati, J. Mol. Biol. **225**, 137 (1992). doi:10.1016/0022-2836(92)91031-J

[47] S. Hajiw, B. Pansu and J.-F. Sadoc, ACS Nano. **9**, 8116 (2015). doi:10.1021/acsnano.5b02216

[48] X. Ye, J. Chen, M. Eric Irrgang, M. Engel, A. Dong, S.C. Glotzer and C.B. Murray, Nat. Mater. **16**, 214 (2017). doi:10.1038/nmat4759

[49] M. Girard, S. Wang, J.S. Du, A. Das, Z. Huang, V.P. Dravid, B. Lee, C.A. Mirkin and M.O. de la Cruz, Science. **364**, 1174 (2019). doi:10.1126/science.aaw8237

[50] K.K. Lachmayr, C.M. Wentz and L.R. Sita, Angew. Chem. Int. Ed. **59**, 1521 (2020). doi:10.1002/anie.201912648

[51] K.K. Lachmayr and L.R. Sita, Angew. Chem. Int. Ed. **59**, 3563 (2020). doi:10.1002/anie.201915416

[52] M.L. Klein, D. Levesque and J.-J. Weis, Phys. Rev. B. **21**, 5785 (1980). doi:10.1103/PhysRevB.21.5785

[53] B.J. Baer and M. Nicol, J. Phys. Chem. **94**, 1073 (1990). doi:10.1021/j100366a009

[54] D. Sihachakr and P. Loubeyre, Phys. Rev. B. **70**, 134105 (2004). doi:10.1103/PhysRevB.70.134105

[55] Y. Akahama, T. Maekawa, T. Sugimoto, H. Fujihisa, N. Hirao and Y. Ohishi, J. Phys. Conf. Ser. **500**, 182001 (2014). doi:10.1088/1742-6596/500/18/182001

[56] R.L. Mills, B. Olinger and D.T. Cromer, J. Chem. Phys. **84**, 2837 (1986). doi:10.1063/1.450310

[57] A.F. Schuch and R.L. Mills, J. Chem. Phys. **52**, 6000 (1970). doi:10.1063/1.1672899

[58] D.T. Cromer, R.L. Mills, D. Schiferi and L.A. Schwalbe, Acta Cryst B. **37**, 8 (1981). doi:10.1107/S0567740881002070

[59] S. Nosé and M.L. Klein, Phys. Rev. Lett. **50**, 1207 (1983). doi:10.1103/PhysRevLett.50.1207

[60] S. Buchsbaum, R.L. Mills and D. Schiferl, J. Phys. Chem. **88**, 2522 (1984). doi:10.1021/j150656a018

[61] D. Tomasino, Z. Jenei, W. Evans and C.-S. Yoo, J. Chem. Phys. **140**, 244510 (2014). doi:10.1063/1.4885724

[62] M. Peterca, M.R. Imam, S.D. Hudson, B.E. Partridge, D. Sahoo, P.A. Heiney, M.L. Klein and V. Percec, ACS Nano. **10**, 10480 (2016). doi:10.1021/acsnano.6b06419

[63] D. Sahoo, M. Peterca, E. Aqad, B.E. Partridge, P.A. Heiney, R. Graf, H.W. Spiess, X. Zeng and V. Percec, ACS Nano. **11**, 983 (2017). doi:10.1021/acsnano.6b07599

[64] D. Sahoo, M. Peterca, E. Aqad, B.E. Partridge, M.L. Klein and V. Percec, Polym. Chem. **9**, 2370 (2018). doi:10.1039/C8PY00187A

[65] N. Huang, M.R. Imam, M.J. Sienkowska, M. Peterca, M.N. Holerca, D.A. Wilson, B.M. Rosen, B.E. Partridge, Q. Xiao and V. Percec, Giant. **1**, 100001 (2020). doi:10.1016/j.giant.2020.100001

[66] V. Percec, D.A. Wilson, P. Leowanawat, C.J. Wilson, A.D. Hughes, M.S. Kaucher, D.A. Hammer, D.H. Levine, A.J. Kim, F.S. Bates, K.P. Davis, T.P. Lodge, M.L. Klein, R.H. DeVane, E. Aqad, B.M. Rosen, A.O. Argintaru, M.J. Sienkowska, K. Rissanen, S. Nummelin and J. Ropponen, Science. **328**, 1009 (2010). doi:10.1126/science.1185547

[67] S.E. Sherman, Q. Xiao and V. Percec, Chem. Rev. **117**, 6538 (2017). doi:10.1021/acs.chemrev.7b00097

[68] M. Peterca, V. Percec, P. Leowanawat and A. Bertin, J. Am. Chem. Soc. **133**, 20507 (2011). doi:10.1021/ja208762u

[69] V. Percec, P. Leowanawat, H.-J. Sun, O. Kulikov, C.D. Nusbaum, T.M. Tran, A. Bertin, D.A. Wilson, M. Peterca, S. Zhang, N.P. Kamat, K. Vargo, D. Moock, E.D. Johnston, D.A. Hammer, D.J. Pochan, Y. Chen, Y.M. Chabre, T.C. Shiao, M. Bergeron-Brlek, S. André, R. Roy, H.-J. Gabius and P.A. Heiney, J. Am. Chem. Soc. **135**, 9055 (2013). doi:10.1021/ja403323y

[70] S. Zhang, H.-J. Sun, A.D. Hughes, B. Draghici, J. Lejnieks, P. Leowanawat, A. Bertin, L. Otero De Leon, O.V. Kulikov, Y. Chen, D.J. Pochan, P.A. Heiney and V. Percec, ACS Nano. **8**, 1554 (2014). doi:10.1021/nn405790x

[71] C. Rodriguez-Emmenegger, Q. Xiao, N.Y. Kostina, S.E. Sherman, K. Rahimi, B.E. Partridge, S. Li, D. Sahoo, A.M.R. Perez, I. Buzzacchera, H. Han, M. Kerzner, I. Malhotra, M. Möller, C.J. Wilson, M.C. Good, M. Goulian, T. Baumgart, M.L. Klein and V. Percec, Proc. Natl. Acad. Sci. U.S.A. **116**, 5376 (2019). doi:10.1073/pnas.1821924116

[72] Q. Xiao, M. Delbianco, S.E. Sherman, A.M.R. Perez, P. Bharate, A. Pardo-Vargas, C. Rodriguez-Emmenegger, N.Y. Kostina, K. Rahimi, D. Söder, M. Möller, M.L. Klein, P.H. Seeberger and V. Percec, Proc. Natl. Acad. Sci. U.S.A. **117**, 11931 (2020). doi:10.1073/pnas.2003938117

[73] S. Li, B. Xia, B. Javed, W.D. Hasley, A. Melendez-Davila, M. Liu, M. Kerzner, S. Agarwal, Q. Xiao, P. Torre, J.G. Bermudez, K. Rahimi, N.Y. Kostina, M. Möller, C. Rodriguez-Emmenegger, M.L. Klein, V. Percec and M.C. Good, ACS Nano. **14**, 7398 (2020). doi:10.1021/acsnano.0c02912

[74] M. Peterca, V. Percec, M.R. Imam, P. Leowanawat, K. Morimitsu and P.A. Heiney, J. Am. Chem. Soc. **130**, 14840 (2008). doi:10.1021/ja806524m

[75] M. Peterca, M.R. Imam, C.-H. Ahn, V.S.K. Balagurusamy, D.A. Wilson, B.M. Rosen and V. Percec, J. Am. Chem. Soc. **133**, 2311 (2011). doi:10.1021/ja110753s

[76] B.M. Rosen, M. Peterca, K. Morimitsu, A.E. Dulcey, P. Leowanawat, A.-M. Resmerita, M.R. Imam and V. Percec, J. Am. Chem. Soc. **133**, 5135 (2011). doi:10.1021/ja200280h

[77] V. Percec, A.E. Dulcey, V.S.K. Balagurusamy, Y. Miura, J. Smidrkal, M. Peterca, S. Nummelin, U. Edlund, S.D. Hudson, P.A. Heiney, H. Duan, S.N. Magonov and S.A. Vinogradov, Nature. **430**, 764 (2004). doi:10.1038/nature02770

[78] J.G. Rudick and V. Percec, New J. Chem. **31**, 1083 (2007). doi:10.1039/b616449h

[79] V. Percec, E. Aqad, M. Peterca, J.G. Rudick, L. Lemon, J.C. Ronda, B.B. De, P.A. Heiney and E.W. Meijer, J. Am. Chem. Soc. **128**, 16365 (2006). doi:10.1021/ja0665848

[80] V. Percec, J.G. Rudick, M. Peterca and P.A. Heiney, J. Am. Chem. Soc. **130**, 7503 (2008). doi:10.1021/ja801863e

[81] V. Percec, J.G. Rudick, M. Peterca, M. Wagner, M. Obata, C.M. Mitchell, W.-D. Cho, V.S.K. Balagurusamy and P.A. Heiney, J. Am. Chem. Soc. **127**, 15257 (2005). doi:10.1021/ja055406w

[82] B.L. Feringa and W.R. Browne, Nat. Nanotechnol. **3**, 383 (2008). doi:10.1038/nnano.2008.194

[83] J.G. Rudick and V. Percec, Acc. Chem. Res. **41**, 1641 (2008). doi:10.1021/ar800086w

[84] C. Roche, H.-J. Sun, P. Leowanawat, F. Araoka, B.E. Partridge, M. Peterca, D.A. Wilson, M.E. Prendergast, P.A. Heiney, R. Graf, H.W. Spiess, X. Zeng, G. Ungar and V. Percec, Nat. Chem. **8**, 80 (2016). doi:10.1038/nchem.2397

[85] B.E. Partridge, L. Wang, D. Sahoo, J.T. Olsen, P. Leowanawat, C. Roche, H. Ferreira, K.J. Reilly, X. Zeng, G. Ungar, P.A. Heiney, R. Graf, H.W. Spiess and V. Percec, J. Am. Chem. Soc. **141**, 15761 (2019). doi:10.1021/jacs.9b08714

[86] L. Wang, B.E. Partridge, N. Huang, J.T. Olsen, D. Sahoo, X. Zeng, G. Ungar, R. Graf, H.W. Spiess and V. Percec, J. Am. Chem. Soc. **142**, 9525 (2020). doi:10.1021/jacs.0c03353

[87] V. Percec, Isr. J. Chem. **60**, 48 (2020). doi:10.1002/ijch.202000004

[88] V. Percec, Q. Xiao, G. Lligadas and M.J. Monteiro, Polymer. **211**, 123252 (2020). doi:10.1016/j.polymer.2020.123252

[89] V. Percec and Q. Xiao, Bull. Chem. Soc. Jpn. **94**, 900 (2021). doi:10.1246/bcsj.20210015

[90] V. Percec and D. Schlueter, Macromolecules. **30**, 5783 (1997). doi:10.1021/ma970157k

[91] Y.K. Kwon, S.N. Chvalun, J. Blackwell, V. Percec and J.A. Heck, Macromolecules. **28**, 1552 (1995). doi:10.1021/ma00109a029

[92] V. Percec, D. Schlueter, G. Ungar, S.Z.D. Cheng and A. Zhang, Macromolecules. **31**, 1745 (1998). doi:10.1021/ma971459p

[93] Y.K. Kwon, S. Chvalun, A.I. Schneider, J. Blackwell, V. Percec and J.A. Heck, Macromolecules. **27**, 6129 (1994). doi:10.1021/ma00099a029

[94] M. Peterca and V. Percec, Science. **330**, 333 (2010). doi:10.1126/science.1196698

[95] V. Percec, M.R. Imam, M. Peterca, D.A. Wilson and P.A. Heiney, J. Am. Chem. Soc. **131**, 1294 (2009). doi:10.1021/ja8087778

[96] V. Percec, M.R. Imam, M. Peterca, D.A. Wilson, R. Graf, H.W. Spiess, V.S.K. Balagurusamy and P.A. Heiney, J. Am. Chem. Soc. **131**, 7662 (2009). doi:10.1021/ja8094944

[97] D. Sahoo, M. Peterca, E. Aqad, B.E. Partridge, P.A. Heiney, R. Graf, H.W. Spiess, X. Zeng and V. Percec, J. Am. Chem. Soc. **138**, 14798 (2016). doi:10.1021/jacs.6b09986

[98] D. Sahoo, M.R. Imam, M. Peterca, B.E. Partridge, D.A. Wilson, X. Zeng, G. Ungar, P.A. Heiney and V. Percec, J. Am. Chem. Soc. **140**, 13478 (2018). doi:10.1021/jacs.8b09174

[99] D.A. Wilson, K.A. Andreopoulou, M. Peterca, P. Leowanawat, D. Sahoo, B.E. Partridge, Q. Xiao, N. Huang, P.A. Heiney and V. Percec, J. Am. Chem. Soc. **141**, 6162 (2019). doi:10.1021/jacs.9b02206

[100] M. Peterca, G. Ungar and V. Percec, Science. **313**, 55 (2006). doi:10.1126/science.1129512

[101] V. Percec, C.-H. Ahn and B. Barboiu, J. Am. Chem. Soc. **119**, 12978 (1997). doi:10.1021/ja9727878

[102] V. Percec, C.-H. Ahn, W.-D. Cho, A.M. Jamieson, J. Kim, T. Leman, M. Schmidt, M. Gerle, M. Möller, S.A. Prokhorova, S.S. Sheiko, S.Z.D. Cheng, A. Zhang, G. Ungar and D.J.P. Yeardley, J. Am. Chem. Soc. **120**, 8619 (1998). doi:10.1021/ja981211v

[103] D.L. Caspar and A. Klug, Cold Spring Harb. Symp. Quant. Biol. **27**, 1 (1962). doi:10.1101/SQB.1962.027.001.005

[104] J. Ropponen, S. Nummelin and K. Rissanen, Org. Lett. **6**, 2495 (2004). doi:10.1021/ol049555f

[105] H. Issidorides and R. Gulen, Org. Synth. **38**, 65 (1958). doi:10.15227/orgsyn.038.0065

[106] H. Ihre, A. Hult, J.M.J. Fréchet and I. Gitsov, Macromolecules. **31**, 4061 (1998). doi:10.1021/ma9718762

[107] I. Buzzacchera, Q. Xiao, H. Han, K. Rahimi, S. Li, N.Y. Kostina, B.J. Toebes, S.E. Wilner, M. Möller, C. Rodriguez-Emmenegger, T. Baumgart, D.A. Wilson, C.J. Wilson, M.L. Klein and V. Percec, Biomacromolecules. **20**, 712 (2019). doi:10.1021/acs.biomac.8b01405

[108] J.S. Moore and S.I. Stupp, Macromolecules. **23**, 65 (1990). doi:10.1021/ma00203a013

[109] W. Cochran, F.H. Crick and V. Vand, Acta Cryst. **5**, 581 (1952). doi:10.1107/S0365110X52001635

[110] L. Pauling and R.B. Corey, Nature. **171**, 59 (1953). doi:10.1038/171059a0

[111] F.H.C. Crick, Acta. Cryst. **6**, 689 (1953). doi:10.1107/S0365110X53001964

[112] E. Moutevelis and D.N. Woolfson, J. Mol. Biol. **385**, 726 (2009). doi:10.1016/j.jmb.2008.11.028

[113] V. Percec, Phil. Trans. R. Soc. A. **364**, 2709 (2006). doi:10.1098/rsta.2006.1848

[114] V. Percec, M.R. Imam, M. Peterca and P. Leowanawat, J. Am. Chem. Soc. **134**, 4408 (2012). doi:10.1021/ja2118267

[115] V. Percec, C.-H. Ahn, T.K. Bera, G. Ungar and D.J.P. Yeardley, Chem. Eur. J. **5**, 1070 (1999). doi:10.1002/(SICI)1521-3765(19990301)5:3 < 1070::AID-CHEM1070 > 3.0.CO;2-9

[116] V. Percec, T.K. Bera, M. Glodde, Q. Fu, V.S.K. Balagurusamy and P.A. Heiney, Chem. Eur. J. **9**, 921 (2003). doi:10.1002/chem.200390114